Attenuation-Difference Tomography of Crosswell Radar Data Using Fresnel Theory

Tim C. Johnson, Partha S. Routh, Michael Knoll and Warren Barrash*
Dept. of Geosciences, Boise State University, Boise, ID

Summary

The traditional approach to attenuation-difference tomography employs the ray approximation where waves are assumed to propagate at infinite frequency. The ray approximation causes significant model error that generates artifacts and loss of resolution in tomographic images. In this paper, we use finite frequency (Fresnel volume) physics to represent wave propagation and propose an efficient method of computing Fresnel volume sensitivities using scattering theory. These sensitivities represent the physics of electromagnetic propagation more accurately than ray theory and thereby provide better data prediction than ray-based sensitivities. We apply this methodology to synthetic and real time-lapse radar attenuation data acquired in a mesoscale hydrogeophysical research site in Boise, Idaho. Both synthetic and field results show that Fresnel theory produces more reliable images of subsurface conductivity changes in comparison to ray theory.

Introduction

Radar attenuation-difference tomography can be used to image spatial and temporal changes in bulk electrical conductivity. Bulk conductivity changes are induced by the movement fluids with different electrical conductivities. Such transport information is typically sensitive to important hydrogeologic properties such as porosity and hydraulic conductivity and can provide valuable information concerning the distribution of these properties. A number of radar attenuation-difference surveys have been conducted in near-surface environments to image fractures (Lane et al., 1999) and to monitor saline tracer tests (Day-Lewis et al., 2002). In both of these applications ray theory was used to represent the wave propagation underlying the inverse reconstruction. The majority of tomographic inversions for velocity or attenuation structure (in both seismic and radar applications) are based on ray theory primarily because ray theory is well understood and is computationally efficient allowing inversions of large data sets.

Several techniques have been developed to estimate the spatial distribution of the sensitivity of seismic arrival time to seismic velocity distributions, which are often referred to as wavepath methods (Luo and Schuster, 1991). Generally, the full acoustic-wave equation is used to derive the wavepath sensitivity distribution associated with a particular source-receiver pair and velocity structure (Vasco and Majer, 1993; Spetzler and Snieder, 2004). Because they are based on a finite-frequency wave equation, the wavepath sensitivities are physically more accurate than rays and include the effects of finite frequency propagation. The benefits of accounting for finite-frequency effects are numerous, including the ability to image smaller scale features and reduce tomographic artifacts.

Fresnel Volume

The Fresnel volume is the region defined by

$$t_{sj} + t_{rj} - t_{sr} \leq \frac{T}{2} \tag{1}$$

where t_{sj} is the travel time from the source to some scattering point in space (cell j in the context of this paper), t_{rj} is the travel time from the same point to the receiver, t_{sr} is the travel time from source to receiver and T is the period of the propagating wave. Energy within the first $T/2$ seconds of the wavelet is only sensitive to points located within the first Fresnel volume because energy scattered from points outside of this volume arrives after time $t_{sr} + T/2$. We define $T/2$ as the time between the first arrival (t_{sr}) and the end of the first pulse (t_{fp}) of the arriving wavelet. In this work we neglect higher order multiple scattering contributions.

For a constant velocity medium the Fresnel volume is an ellipsoid with focal points at source and receiver positions. As frequency decreases the Fresnel zone widens indicating that the energy contained in the first pulse is sensitive to a wider region in space. As frequency increases toward infinity the period approaches zero and the Fresnel zone becomes very narrow indicating that the first pulse is sensitive only to the locus of points lying on a curve between the source and receiver as in the ray approximation. We assume a constant velocity medium so that rays are straight and Fresnel volumes are ellipsoidal. The straight-ray approximation is valid in many saturated shallow subsurface environments because velocity contrasts tend to be weak and source receiver distances are small which limits ray bending. However, Fresnel volumes can also be computed for heterogeneous velocity media (Spetzler and Snieder, 2004).

Attenuation Difference Data

Consider that the time domain trace of the vertical component of the electric field (E_z) corresponding to the source-receiver orientation i is given by $e_{a,i}$. A trace with the same acquisition geometry collected at some later time t_b, when an electrically anomalous fluid has invaded the region between the source and receiver, is labeled $e_{b,i}$. If the fluid is conductive, the amplitude of $e_{a,i}$ will be

greater than the amplitude of $e_{b,i}$ because EM wave attenuation increases with conductivity. In low loss conditions, the relationship between the natural logarithm of EM amplitude and bulk conductivity is approximately linear. Thus we can define the attenuation-difference data as

$$\delta D_i = \ln\left(\int_{t_{sr}}^{t_{fp}} e_{b,i}^2(t)dt\right) - \ln\left(\int_{t_{sr}}^{t_{fp}} e_{a,i}^2(t)dt\right) \quad (2)$$

where t_{sr} is the first arrival time for traces $e_{a,i}$ and $e_{b,i}$, and t_{fp} is the time to the end of the first pulse or the first zero crossing after t_{sr}. The kinematic parts of the wave equation are equal for both times; only wave amplitudes are affected. Under this assumption, the integration limits in eq. 2 are equal for each trace.

To construct the forward model, let the conductivity distribution at times t_a and t_b be denoted by $\sigma_a(\mathbf{r})$ and $\sigma_b(\mathbf{r})$, such that $\sigma_b(\mathbf{r}) = \sigma_a(\mathbf{r}) + \delta\sigma(\mathbf{r})$ then Eq. 2 is given by .

$$\delta D_i = \ln\left(\int_{t_{sr}}^{t_{fp}} e_i^2\left(\sigma_a(\mathbf{r}) + \delta\sigma(\mathbf{r}), t\right)dt\right) - \quad (3a)$$

$$\ln\left(\int_{t_{sr}}^{t_{fp}} e_i^2\left(\sigma_a(\mathbf{r}), t\right)dt\right). \quad (3b)$$

If we represent the integrals by $F_i(\sigma(\mathbf{r})) = \int_{t_{sr}}^{t_{fp}} e_i^2\left(\sigma(\mathbf{r}), t\right)dt$, then Eq. 3 can be written (Johnson et al., 2005)

$$\delta D_i = \left\langle \frac{1}{F_i\left(\sigma_a(\mathbf{r})\right)} \frac{\partial F_i\left(\sigma_a(\mathbf{r})\right)}{\partial \sigma_a(\mathbf{r})}, \delta\sigma(\mathbf{r}) \right\rangle \quad (4)$$

Where $\langle\cdot,\cdot\rangle$ denotes the inner product in the spatial domain and $\partial F_i\left(\sigma_a(\mathbf{r})\right)/\partial\sigma_a(\mathbf{r})$ are Frechet derivatives. Discretizing the medium into cells of volume v_j with conductivity $\delta\sigma_j$ allows us to write Eq(4 as

$$\delta D_i = \sum_{j=1}^{N} J_{ij}^F \delta\sigma_j \quad (5)$$

where $J_{ij}^F = \partial \ln\left(F_i\left(\sigma_a(\mathbf{r})\right)\right)/\partial\sigma_j$. Eq.5 is the discretized forward model for Fresnel volume attenuation-difference tomography. Errors in the physics represented by J^F arise primarily due to the truncation of higher order terms which neglects the effects of multiple scattering. This effect is evident in the expression for J_{ij}^F which is the sensitivity of the log first pulse energy of $e_i(\sigma_a(\mathbf{r}))$ to a single scatterer $\delta\sigma_j$.

We compute J_{ij}^F with the forward finite difference operator given by

$$J_{ij}^F = \frac{\ln\left(\int e_i^2\left(\sigma_a(\mathbf{r}) + \delta\sigma_j\right)dt\right) - \ln\left(\int e_i^2\left(\sigma_a(\mathbf{r})\right)dt\right)}{\delta\sigma_j}. \quad (6)$$

We solve for $e_i\left(\sigma_a(\mathbf{r})\right)$ and $e_i\left(\sigma_a(\mathbf{r}) + \delta\sigma_j\right)$ using scattering theory and numerically compute the integrations in Eq. 6. The background field $e_i\left(\sigma_a(\mathbf{r})\right)$ is computed assuming constant $\sigma_a(\mathbf{r})$ and $e_i\left(\sigma_a(\mathbf{r}) + \delta\sigma_j\right)$ is computed using the Born approximation.

Fresnel Volume Sensitivities

To solve Eq. 6 we are required to compute the background and scattered fields using the Helmholtz equation. The background field is solved using the whole space Green's function in a homogeneous medium and the scattered field solution is solved using a first order scattering solution, which is effectively the Born approximation. Details of the derivation is presented in Johnson et. al (2005). The background electric field is represented by

$$E_0(\mathbf{r},\omega) = \frac{i\omega\mu_0}{4\pi}\frac{1}{|\mathbf{r}-\mathbf{r}_0|}S(\omega)\mathbf{e}^{-\mathbf{i}k|\mathbf{r}-\mathbf{r_0}|} \quad (7)$$

and the total field solution due to a single scatterer is given by

$$E(r,\omega) = \frac{i\omega\mu_0}{4\pi}\frac{1}{|\mathbf{r}-\mathbf{r}_0|}S(\omega)\mathbf{e}^{-\mathbf{i}k|\mathbf{r}-\mathbf{r_0}|} - \quad (8a)$$

$$\frac{\omega^2\mu_0^2 v_j\delta\sigma_j}{16\pi^2|\mathbf{r}-\mathbf{r_j}||\mathbf{r}_j-\mathbf{r}_0|}\mathbf{e}^{-ik(|\mathbf{r}-\mathbf{r_j}|+|\mathbf{r_j}-\mathbf{r_0}|)}S(\omega). \quad (8b)$$

Eq. 8 is the fundamental equation used in computing the EM field due to a conductive perturbation in a homogeneous medium. It is the total field solution for a single scatterer under the Born approximation. We compare the solution from scattering theory with the full-waveform finite difference solution (Holliger and Bergmann, 2002) shown in Fig. **??**4}. The scattering solution matches well with the finite difference solution. The effect of radiation pattern on sensitivity is shown in Fig. **??**7}. The distortion of the sensitivities for the anisotropic radiation pattern indicate the importance of radiation patterns in attenuation-difference data. Figure

Inversion of Synthetic Data

Figures 3 and 4 shows the results of a synthetic data inversion using singular value decomposition (SVD). The Fresnel and ray theory solutions are presented at different truncation indexes. The truncation index corresponding to the noise level in the data is close to 160 for the Fresnel zone case and 200 for the straight ray case. Therefore the images at 160 and 200 are the appropriate solutions for the Fresnel zone and straight ray inversions respectively. Comparing the results we notice a significant improvement in the recovered bulk conductivity changes using the Fresnel zone approach. The top anomalous zone is poorly recovered using ray theory and the overall amplitude recovery is much lower compared to the Fresnel inversion results.

Inversion of Field Data at BHRS

Figure 5 shows the tomographic images constructed using ray theory and Fresnel theory of the bromide tracer plume acquired during a tracer test at the Boise Hydrogeophysical Research Site (BHRS) (Barrash et al., 2003; Goldstein, 2004). The data were acquired 9 days after a bromide tracer injection and image plane is approximately 4.5 meters from the injection well. The plume is moving approximately perpendicular to the plane (i.e. coming out of the page). The source receiver configurations are evenly spaced at 20 cm intervals in each well for a total of 2350 source receiver pairs (100 MHz) data. The inversions were constructed using first spatial derivative regularization and solved using LSQR. The appropriate regularization weighting for each case was determined with the L-curve technique, and each solution has approximately the same data residual norm. The results are very similar to what the synthetic inversion indicates. Namely, the Fresnel volume inversions are much better localized and predict higher conductivity changes. (i.e. note the scale differences).

Conclusions

In this paper we demonstrate that using finite-frequency approximations provide improved images of bulk conductivity in the subsurface. The sensitivities computed using Fresnel theory are similar to the the full-waveform sensitivities.Interestingly, the Fresnel volume sensitivities are zero along the correspoding ray path. We include radiation pattern effects and have shown that sensitivity distributions are distorted by anisotropic radation patterns. We demonstrate using synthetic and real examples that Fresnel volume sensitivities approximated with scattering theory can provide inverse estimates that are significantly more localized and accurate than the ray theory counterparts.

Acknowledgments

Many thanks to Klaus Holliger for graciously allowing us to employ his full-waveform finite difference modelling code in this project. Funding for this work was provided by the Inland Northwest Research Alliance (Ph.D. fellowship for TJ), Bechtel BWXT Idaho, LLC (contract 00036570), and EPA grant X-970085-01-0. Computations were performed on the geophysical computing system (NSF-EPSCoR grant # EPS0132626) at CGISS and the Beowulf cluster at Boise State University (NSF-Major Research Infrastructure Award # 0321233). We thank James Nelson for his assistance with the parallel computers.

References

Barrash, W., Knoll, M., Hyndman, D., Clemo, T., Reboulet, E., and Hausrath, E., 2003, Tracer/time-lapse radar imaging test at the boise hydrogeophysical research site: Proceedings of SAGEEP, pages 163–174.

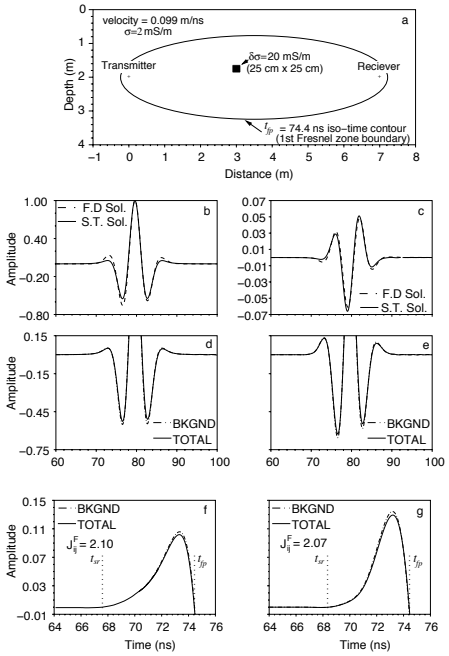

Fig. 1: Scattering theory (S.T.) and finite difference (F.D.) solution comparisons. a) Source position, receiver position, scattering size, magnitude, and Fresnel volume boundary. b) Scattering theory and finite difference background solutions $e_i(\sigma_a(\mathbf{r}))$. c) Scattering theory and finite difference scattered solutions $e_{1i}(\sigma_a(\mathbf{r}) + \delta\sigma_j)$. d) Scattering theory background and total field solutions. e) Finite difference background and total field solutions. f) Scattering theory background and total field first pulse, integration limits and sensitivity estimation. g) Finite difference background and total field first pulse, integration limits and sensitivity estimation. The sensitivity estimations are comparable in each case.

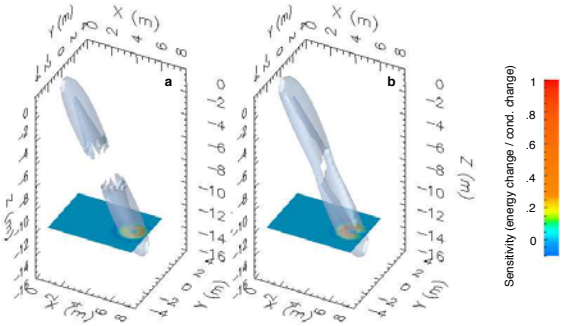

Fig. 2: 3D scattering theory Fresnel volumes. Isosurfaces at a sensitivity value of 1. Source (x,y,z) = (1,0,-1)m. Receiver (x,y,z) = (7,0,-15). Cross section is z-normal at z = -12 m. a) Sensitivities assuming isotropic radiation pattern. b) Sensitivities assuming dipole type source and receiver radiation patterns.

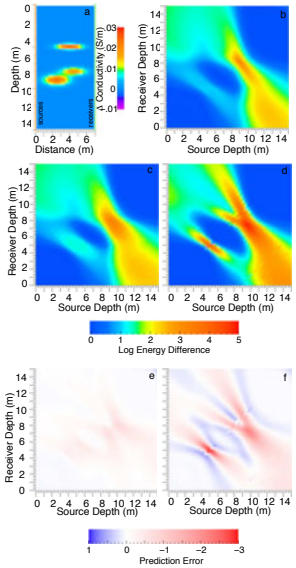

Fig. 3: Fresnel zone and ray-based data predictions. Background conductivity is 0.002 S/m. a) The conductivity model $\delta\sigma(\mathbf{r})$. Borehole separation is 7 m. Boreholes are 15 m deep with sources and receivers every 0.25 m. b) Finite difference generated data (δD_i) cross-plot. c) Scattering theory data prediction (δD_i^F) cross-plot. d) Ray-based data prediction (δD_i^S) cross-plot. e) Scattering theory prediction error ($\delta D_i^F - \delta D_i$). f) Ray-based model prediction error ($\delta D_i^S - \delta D_i$).

Day-Lewis, F., Harris, J., and Gorelick, S., 2002, Time-lapse inversion of crosswell radar data: Geophysics, **69**, no. 6, 1740–1752.

Goldstein, S., 2004, Cross-well radar attenuation-difference tomography to monitor bromide tracer test: Masters Thesis, Boise State University.

Holliger, K., and Bergmann, T., 2002, Numerical modeling of borehole georadar data: Geophysics, **67**, no. 04, 1249–1257.

Johnson, T. C., Routh, P. S., and Knoll, M. D., 2005 Fresnel volume georadar attenuation differenc tomography: Geophy. J. Inter. (accepted).

Lane, J., Wright, D., and Haeni, P., 1999, Borehole radar tomography using saline tracer injections to image fluid flow in fractured rock: Borehole radar tomography using saline tracer injections to image fluid flow in fractured rock:, USGS Toxic Substances Hydrology Meeting, March 8-12, Charleston, SC.

Luo, Y., and Schuster, G. T., 1991, Wave-equation traveltime inversion: Geophysics, **56**, no. 05, 645–653.

Spetzler, J., and Snieder, R., 2004, The fresnel volume and transmitted waves: Geophysics, **69**, no. 3, 653–663.

Vasco, D., and Majer, E., 1993, Wavepath traveltime tomography: Geophysical Journal International, **115**, 1055–1069.

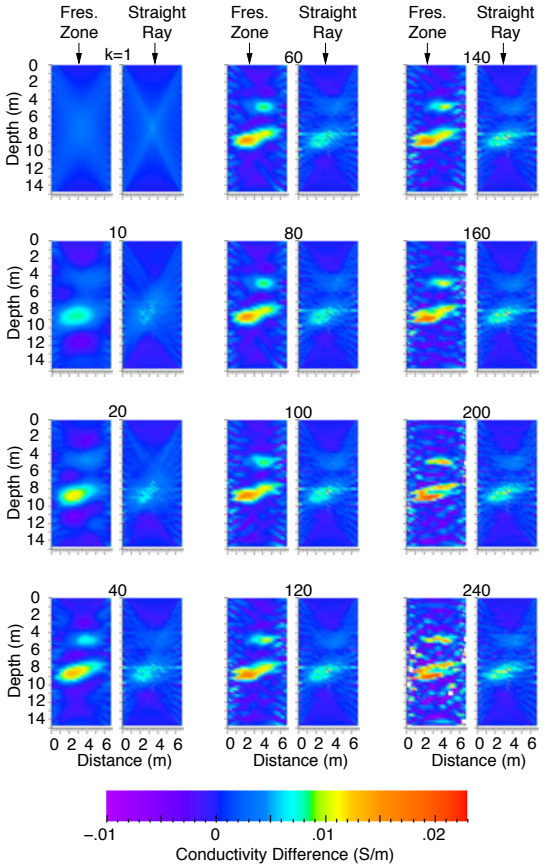

Fig. 4: Fresnel zone and straight-ray SVD Solutions vs. truncation index. for the synthetic example

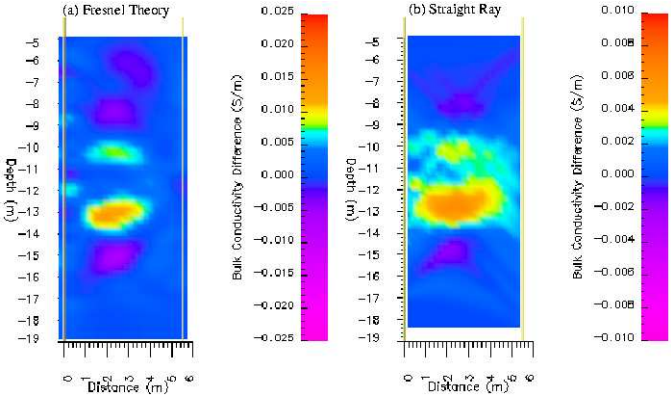

Fig. 5: Field data example: Inverted image of bulk conductivity change of BHRS data using (a) Fresnel and (b) Ray theory approach.The color scale in (a) is from -0.025 to 0.025 and in (b) is from -0.01 to 0.01

EDITED REFERENCES

Note: This reference list is a copy-edited version of the reference list submitted by the author. Reference lists for the 2005 SEG Technical Program Expanded Abstracts have been copy edited so that references provided with the online metadata for each paper will achieve a high degree of linking to cited sources that appear on the Web.

REFERENCES

Barrash, W., M. Knoll, D. Hyndman, T. Clemo, E. Reboulet, and E. Hausrath, 2003, Tracer/time-lapse radar imaging test at the Boise hydrogeophysical research site: Proceedings of SAGEEP, 163–174.

Day-Lewis, F., J. Harris, and S. Gorelick, 2002, Time-lapse inversion of crosswell radar data: Geophysics, **69**, 1740–1752.

Goldstein, S., 2004, Cross-well radar attenuation-difference tomography to monitor bromide tracer test: M.S. thesis, Boise State University.

Holliger, K., and T. Bergmann, 2002, Numerical modeling of borehole georadar data: Geophysics, **67**, 1249–1257.

Johnson, T. C., P. S. Routh, and M. D. Knoll, 2005, Fresnel volume georadar attenuation difference tomography: Geophysical Journal International (accepted).

Lane, J., D. Wright, and P. Haeni, 1999, Borehole radar tomography using saline tracer injections to image fluid flow in fractured rock: USGS Toxic Substances Hydrology Meeting.

Luo, Y., and G. T. Schuster, 1991, Wave-equation traveltime inversion: Geophysics, **56**, 645–653.

Spetzler, J., and R. Snieder, 2004, The fresnel volume and transmitted waves: Geophysics, **69**, 653–663.

Vasco, D., and E. Majer, 1993, Wavepath traveltime tomography: Geophysical Journal International, **115**, 1055–1069.